LETTERS
https://doi.org/10.1038/s41565-020-0697-2
nature nanotechnology

Radiative Auger process in the single-photon limit

Matthias C. Löbl[1]✉, Clemens Spinnler[1], Alisa Javadi[1], Liang Zhai[1], Giang N. Nguyen[1,2], Julian Ritzmann[2], Leonardo Midolo[3], Peter Lodahl[3], Andreas D. Wieck[2], Arne Ludwig[2] and Richard J. Warburton[1]

In a multi-electron atom, an excited electron can decay by emitting a photon. Typically, the leftover electrons are in their ground state. In a radiative Auger process, the leftover electrons are in an excited state and a redshifted photon is created[1–4]. In a semiconductor quantum dot, radiative Auger is predicted for charged excitons[5]. Here we report the observation of radiative Auger on trions in single quantum dots. For a trion, a photon is created on electron–hole recombination, leaving behind a single electron. The radiative Auger process promotes this additional (Auger) electron to a higher shell of the quantum dot. We show that the radiative Auger effect is a powerful probe of this single electron: the energy separations between the resonance fluorescence and the radiative Auger emission directly measure the single-particle splittings of the electronic states in the quantum dot with high precision. In semiconductors, these single-particle splittings are otherwise hard to access by optical means as particles are excited typically in pairs, as excitons. After the radiative Auger emission, the Auger carrier relaxes back to the lowest shell. Going beyond the original theoretical proposals, we show how applying quantum optics techniques to the radiative Auger photons gives access to the single-electron dynamics, notably relaxation and tunnelling. This is also hard to access by optical means: even for quasi-resonant *p*-shell excitation, electron relaxation takes place in the presence of a hole, complicating the relaxation dynamics. The radiative Auger effect can be exploited in other semiconductor nanostructures and quantum emitters in the solid state to determine the energy levels and the dynamics of a single carrier.

Auger processes are a well-known phenomenon in atoms[6,7]. Non-radiative Auger processes involving continuum states have been observed in several solid-state systems: quantum dots[8], two-dimensional materials[9], colour centres[10] and semiconductor lasers[11]. As originally predicted for atoms, an Auger process can also take place in connection with a radiative transition[3,4]. In such a radiative Auger process, part of the available energy is transferred to another electron and the emitted photon is correspondingly redshifted. The radiative Auger process has been observed in X-ray spectra[1,2]. The so-called electron shake-off process has a similar physical origin[12]. At optical frequencies, the radiative Auger process has been described in ensembles of donors[13] and as a so-called shake-up process in the Fermi sea[14–16], a many-particle effect. On a single-photon emitter or in a few-electron configuration, the radiative Auger process has not been observed.

We observe the radiative Auger process in two different systems: (1) a self-assembled InGaAs quantum dot (QD) in GaAs grown in the Stranski–Krastanov mode[5]; and (2) a GaAs QD in AlGaAs grown by infilling of droplet-etched nanoholes[17]. We resonantly excite the negative trion (X^{1-}) of a QD with a narrow-bandwidth laser. In both QD systems, the charge state of the QD is precisely controlled via Coulomb blockade[18]. We collect the emission of the QD and resolve it spectrally, as schematically shown in Fig. 1a. Figure 1b shows the result of such a measurement for an InGaAs QD. The main peak at photon energy $E \approx 1.321$ eV is the resonance fluorescence of the trion. This spectrally narrow emission is accompanied by a longitudinal acoustic (LA)-phonon sideband on the red side[19–21]. In addition, we observe two weak emission lines, redshifted by ~18 meV from the main fluorescence peak. In the following, we show that these emission lines originate from a radiative Auger process as illustrated in Fig. 1c: an electron and a hole recombine optically, and with a small probability, the second electron is promoted to an excited state, the *p* shell of the QD. In the case of resonance fluorescence, in contrast, the optical recombination of the trion leaves behind a single electron in the ground state (the *s* shell of the QD).

Several observations substantiate the interpretation that the two redshifted lines originate from a radiative Auger process. First, the Auger lines disappear on removing the additional electron—they are absent in the emission spectrum of the neutral exciton, X^0 (Supplementary Fig. 1). Second, the redshifted emission lines appear only when the laser is in resonance with the QD (Fig. 1b). Third, the time-resolved cross-correlation between the radiative Auger emission and the resonance fluorescence (Fig. 1d,e) shows a pronounced anti-bunching at zero time delay. This measurement demonstrates that the different emission lines originate from the same QD. The emitter produces either a resonance fluorescence photon or a radiative Auger photon, but never two photons at the same time. Finally, to prove that the radiative Auger process leaves an electron in a higher shell, we measure the optical emission as a function of the magnetic field (Faraday geometry). The magnetic field dispersion of the radiative Auger emission is shown in Fig. 2a,b for an InGaAs QD and in Fig. 2c,d for a GaAs QD. At high magnetic fields, the two redshifted emission lines, which are the closest in energy to the resonance fluorescence, have a dispersion of $\pm \frac{1}{2}\hbar\omega_c$ (where $\omega_c = \frac{eB}{m^*}$ is the cyclotron frequency, m^* is the electron effective mass, e is the elementary charge, B is the magnetic field and $\hbar$ is the reduced Planck constant). This magnetic field dispersion shows that the emission is connected to an energy transfer to the *p* shells. More generally, the strong magnetic field dispersion of the radiative Auger emission arises because the magnetic field creates an additional orbital confinement, which leads to a strong magnetic field dependence of higher QD shells[22–24]. The magnetic field dependence is important to distinguish radiative Auger emission from phonon-related features.

The separation between resonance fluorescence and radiative Auger emission corresponds to the single-particle splittings. The radiative Auger lines, therefore, allow the single-particle spectrum of a QD to be determined with high precision. At zero magnetic

[1]Department of Physics, University of Basel, Basel, Switzerland. [2]Lehrstuhl für Angewandte Festkörperphysik, Ruhr-Universität Bochum, Bochum, Germany. [3]Niels Bohr Institute, University of Copenhagen, Copenhagen, Denmark. ✉e-mail: matthias.loebl@unibas.ch

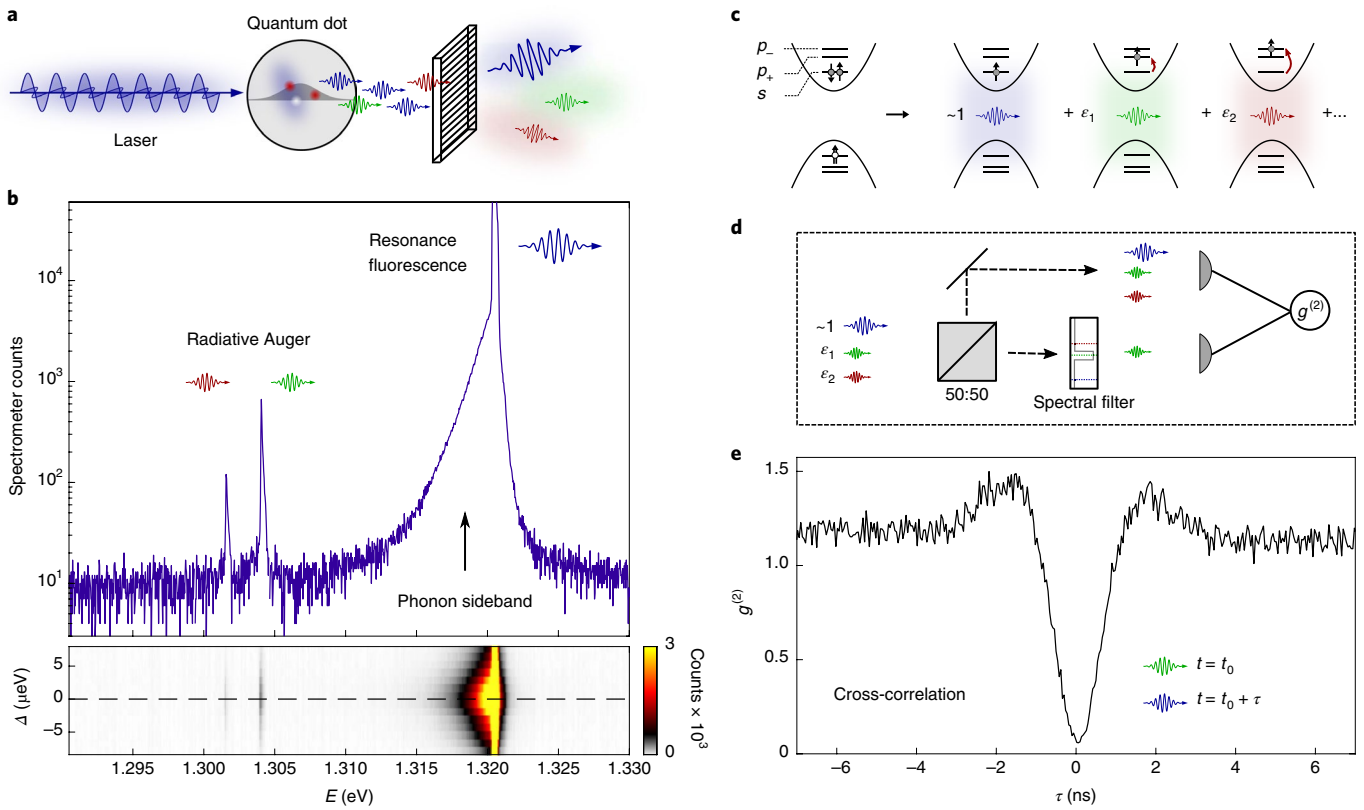

Fig. 1 | Observation of a radiative Auger process on a single QD. a, Schematic of the experimental setup: the QD is resonantly excited with a narrow-bandwidth laser, and its emission is spectrally resolved. **b**, Upper panel, emission spectrum of the negative trion (X^{1-}) in an InGaAs QD under resonant excitation (temperature 4.2 K). The strong peak at $E \approx 1.321$ eV is the resonance fluorescence, which is surrounded by a broad LA-phonon sideband. Redshifted by ~18 meV there are two additional emission lines, stemming from the radiative Auger process. Lower panel, the QD can be tuned in and out of the resonance with the laser by exploiting the d.c. Stark effect via a gate voltage, V_g. The spectrum shown in the upper panel is measured at zero detuning, Δ, between the QD and laser (dashed line). Resonance fluorescence and radiative Auger are maximum when the QD and laser are in resonance ($\Delta = 0$). (See also Supplementary Note V.) **c**, Mechanism of the radiative Auger process: with a probability close to one, the trion recombination results in an emission of a resonant photon and leaves the remaining electron in the ground state (*s* shell). With small probabilities $|\epsilon_1|^2$ and $|\epsilon_2|^2$, the remaining electron is promoted into one of the *p* shells, and the photon is consequently redshifted. **d**, Setup for the cross-correlation between the radiative Auger emission and the resonance fluorescence. The delay τ corresponds to the duration between the arrival of a resonant photon on detector 2 after the detection of an Auger photon on detector 1 (at time t_0). **e**, Cross-correlation measurement between the radiative Auger emission and the resonance fluorescence. The strong anti-bunching at zero time delay proves that both emission lines originate from the same emitter.

field ($B = 0$ T), there is a splitting between the two *p*-shell-related Auger lines, revealing an asymmetry of the QD. This asymmetry lifts the fourfold degeneracy of the *p* shells into two doublets at zero magnetic field. For both types of QDs, we also observe radiative Auger emission at even lower energies (Fig. 2a,c). These emission lines correspond to a radiative Auger process involving *d* shells (Fig. 2e). At high magnetic fields, the upper *p* shell (p_-) shows an anti-crossing with the lowest *d* shell (d_+). For the GaAs QD, we even observe radiative Auger emission lines involving all three *d* shells. For the InGaAs QD, the d_+ shell is only visible in the radiative Auger emission when it is coupled to the p_- shell. For both types of QDs, we model the dispersion of the emission lines by the Fock–Darwin spectrum[23,24] (details in Supplementary Note I). The model assumes a harmonic confinement potential and matches well for the lower QD shells (Fig. 2a,c). Differences between the model and data (for example, for the *d* shells) reveal the deviation from a harmonic confinement potential towards higher single-particle energy.

For a rotationally symmetric confinement potential, angular momentum is a good quantum number such that promotion of the Auger electron to the d_0 shell is possible, but promotion to the other *p* and *d* shells is forbidden. In practice, we find that the radiative Auger involving the *p* shells is relatively strong and that the intensity of these processes is not strongly dependent on the magnetic field. Besides, the *p* shells are not degenerate at zero magnetic field. These observations show that angular momentum is not a good quantum number. However, we do not observe Zeeman splittings in the radiative Auger lines, which shows that the processes are spin-conserving. Spin is a good quantum number; equivalently, spin–orbit interactions of the electron states are weak.

There are several additional redshifted emission lines that are not related to electron shells or continuum states (Fig. 2a,b): an emission redshifted by ~36 meV (labelled LO in Fig. 2b,d) corresponds to an optical recombination along with the creation of a longitudinal optical (LO) phonon (Fig. 2f). The magnetic field dispersion is weak and follows the QD *s* shell—no higher QD shells are involved. At lower photon energies, even the LO-phonon replica of the radiative Auger emission is visible (labelled LO + $p_\pm$ in Fig. 2b, schematic in Fig. 2g). In this case, Auger carrier excitation into *p* shells and LO-phonon creation occur simultaneously with the optical recombination. The identification of these lines is confirmed by the magnetic field dispersion, which equals the dispersion of the radiative Auger emission (Fig. 2b).

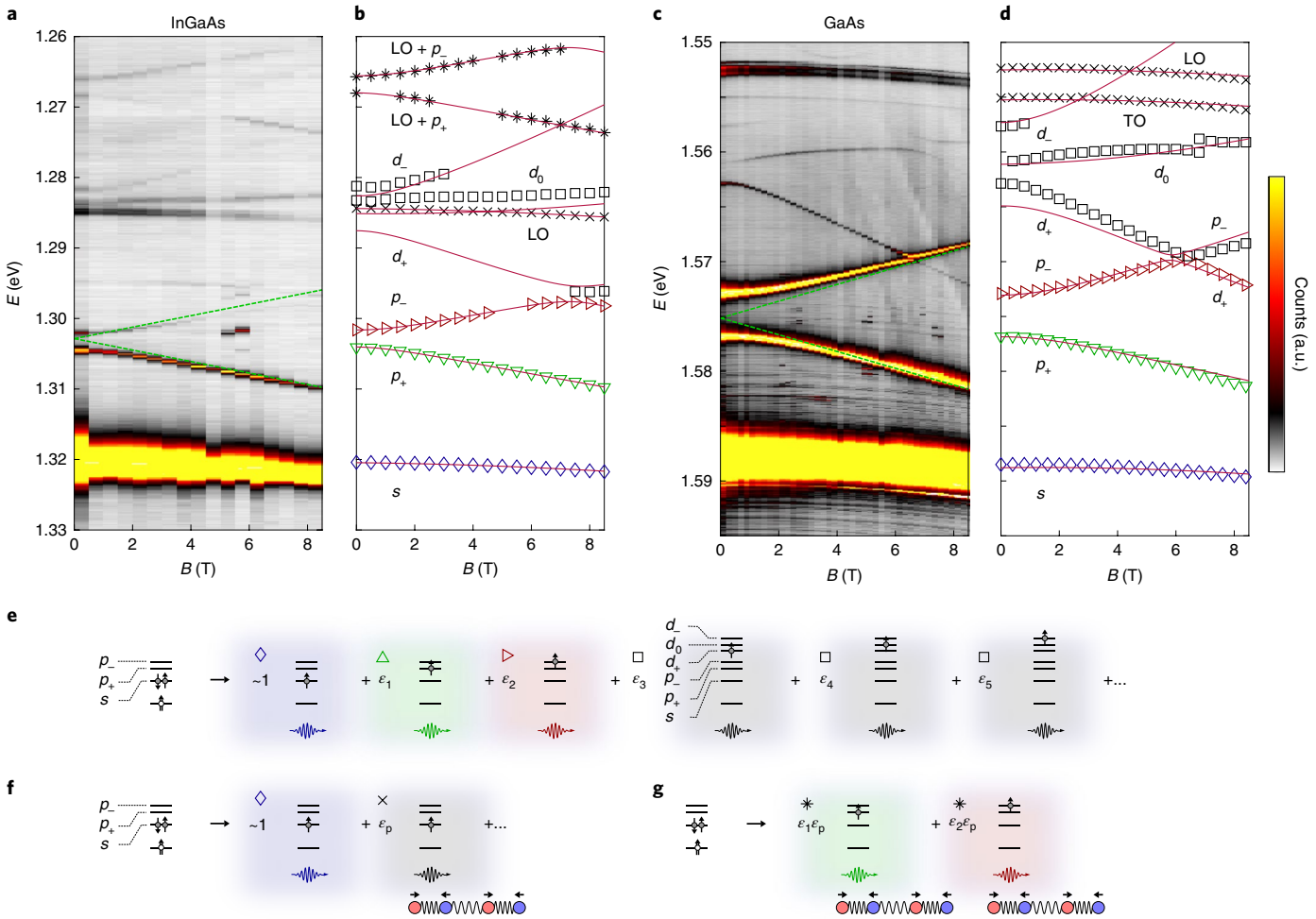

Fig. 2 | Magnetic field dispersion of the radiative Auger emission. a, Emission spectrum under resonant excitation as a function of the magnetic field measured on an InGaAs QD. The two green lines indicate the radiative Auger emission where one electron is promoted into the *p* shells. This emission follows a dispersion of $\sim \pm\frac{1}{2}\hbar\omega_c$, with $m^* \approx 0.071 m_e$ (m_e, electron mass; *s*-to-*p*-splitting: $\hbar\omega_0 \approx 17.7$ meV; further parameters in Supplementary Table 2). **b**, Magnetic field dispersion of the radiative Auger emission. The emission lines above the *s* shell can be well described by the Fock–Darwin spectrum. The red lines represent a fit of our analytical model of the radiative Auger emission. **c**, Radiative Auger emission as a function of the magnetic field measured on a GaAs QD ($m^* \approx 0.076 m_e$, $\hbar\omega_0 \approx 13.8$ meV). **d**, Magnetic field dispersion of the radiative Auger emission for the GaAs QD. **e**, Schematics of the radiative Auger process involving both *p* and *d* shells. **f**, Optical recombination involving the creation of an LO or a transverse optical (TO) phonon. We note that this process is observed for the trion and the neutral exciton (Supplementary Fig. 1). $|\epsilon_p|^2$ labels the probability for the process involving the LO phonon. **g**, Schematics of the radiative Auger process involving both carrier excitation to the *p* shell and the creation of a phonon.

We turn to the dynamics of the radiative Auger process, that is, the dynamics of the electron left in an excited state after a radiative Auger process. Detecting a photon from a radiative Auger process projects the Auger electron into one of the excited electron states. The dynamics of this single electron can be investigated by determining the time of subsequent emission events. The experiment involves measuring the photon correlation function, $g^{(2)}(\tau)$, with high precision in the delay τ. We compare the autocorrelation of the resonance fluorescence (Fig. 3a) to the cross-correlation between the radiative Auger emission and the resonance fluorescence (Fig. 3b). This comparison provides immediate insight into the carrier relaxation mechanism following the radiative Auger process. The corresponding $g^{(2)}$ measurements are shown in Fig. 3c.

The autocorrelation (blue curve) shows a very pronounced anti-bunching ($g^{(2)} << 1$) at zero time delay, proving the single-photon nature of the resonance fluorescence. The anti-bunching is surrounded by a bunching ($g^{(2)} > 1$) at a non-zero time delay. This effect is caused by the onset of Rabi oscillations under strong resonant driving. The cross-correlation (green curve) differs from the autocorrelation in two aspects: The $g^{(2)}(\tau)$ is a slightly asymmetric function of τ and has a time offset towards positive τ. We can explain these features (see fit in Fig. 3d) with the mechanism shown in Fig. 3e: after the emission of a radiative Auger photon, the second electron is located in a higher shell. Before re-excitation of the trion can take place, this electron has to relax down to the *s* shell—in contrast to the resonance fluorescence where re-excitation is immediately possible. By comparing auto- and cross-correlation, we determine the relaxation time for an isolated electron to be $\tau_p \approx 85$ ps. The timescale of the electron relaxation is comparable to numbers reported for weak non-resonant excitation[25,26]. The relaxation is probably caused by a multiphonon emission process[27]. We stress the advantage of the present method: the radiative Auger process leaves only a single electron in a higher shell. In contrast to non-resonant excitation, all other carriers have disappeared and the relaxation of the electron can be investigated independently of other relaxation mechanisms.

The asymmetry of the cross-correlation measurement can be explained by ionization of the QD following the radiative Auger

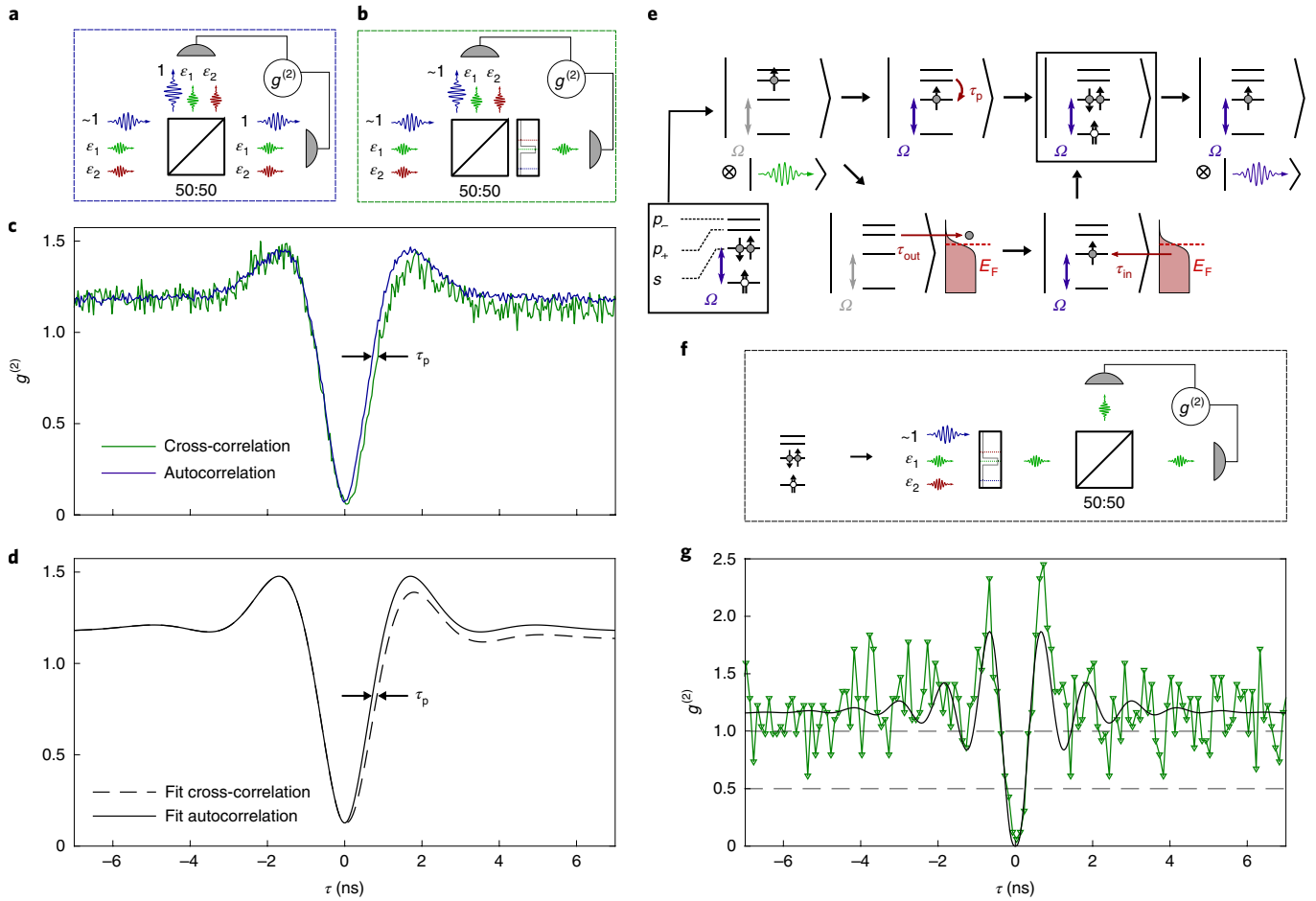

Fig. 3 | Time-resolved correlation measurements. a, Schematic of the measurement to determine the autocorrelation of the resonance fluorescence from a QD. The signal is split by a 50:50 beamsplitter; photon arrival times are recorded on two single-photon detectors ($g^{(2)}$ measurement). **b**, Schematic of the cross-correlation measurement between resonance fluorescence and radiative Auger emission. The Auger emission is spectrally filtered to remove all resonant photons. **c**, Cross-correlation between the resonance fluorescence and the radiative Auger emission (green), measured on the InGaAs QD shown in Fig. 1. An autocorrelation of the resonance fluorescence (blue) is shown for comparison. A time offset of $\tau_p \approx 85$ ps between the autocorrelation and the cross-correlation is a measure of the relaxation time of a single electron from the *p* shell to the *s* shell. **d**, Fits to the auto- and cross-correlation measurements (parameters listed in Supplementary Table 3). **e**, Model for the dynamics connected to the radiative Auger process. After the radiative Auger excitation, the second electron occupies the *p* shell of the QD. When the electron occupies the *p* shell rather than the *s* shell, the Coulomb interactions are different, tuning the *s*-to-*s* transition out of resonance with the laser (Ω, Rabi frequency). The QD cannot be re-excited until the electron has relaxed to the *s* shell. There are two relaxation channels: a direct relaxation to the *s* shell on a timescale τ_p; and ionization of the QD by tunnelling from the *p* shell to the Fermi reservoir (E_F, Fermi energy), of the back gate (τ_{out}) followed by slower tunnelling from the Fermi reservoir to the *s* shell (τ_{in}). After relaxation, the QD is re-excited by the laser. **f**, Schematic setup for the autocorrelation measurement of the radiative Auger emission. The radiative Auger signal is split and sent to two single-photon detectors. **g**, Autocorrelation of the radiative Auger process involving the lower-energy *p* shell (green). The solid black line is a model where all parameters are identical to the simulation of the cross-correlation (see **d** and Supplementary Note III). Only the Rabi frequency is higher compared with the cross-correlation measurement.

emission. In a higher shell, the electron has an enhanced tunnelling rate out of the QD[28]. Following very fast relaxation down to the Fermi energy, tunnelling back into the *s* shell of the QD takes about ten times longer, and the QD is ionized for a finite time. We estimate the corresponding tunnelling times by modelling the auto- and cross-correlation measurements. The full model and the fit results are given in Supplementary Note VI; the fits describe the experimental data well (Fig. 3d).

Finally, we perform the first autocorrelation measurement of the radiative Auger emission. For this measurement, all the resonance fluorescence is filtered out (Fig. 3f). To maximize the count rate of the weak radiative Auger emission, we use a higher Rabi frequency compared with the cross-correlation measurement. The autocorrelation measurement is shown in Fig. 3g. At zero time delay, there is a clear anti-bunching in the $g^{(2)}$ measurement, which proves the single-photon nature of the emission connected to the radiative Auger process. At non-zero time delay, the onset of Rabi oscillations in the *s*-to-*s* transition is visible as a photon bunching of the radiative Auger emission. Both features are well described by our model (Supplementary Note III).

The radiative Auger process takes place because the interactions between the carriers forming the trion change the eigenfunctions of the system (Supplementary Note II). In a single-particle basis, the initial state contains admixtures of Slater determinants[29,30] of higher single-particle shells. The optical recombination removes an electron–hole pair from the initial trion state, leading to a final state that is a superposition of single-electron single-particle states. Every state in that superposition consists of an electron in a particular

shell along with a photon of a certain energy. Since the initial state is always the same, the energy separations between the different emission lines correspond to precise single-particle splittings. The ratio of radiative Auger emission and resonance fluorescence reflects the expansion of the trion state in single-particle states. Compared with the resonance fluorescence, the radiative Auger emission is weaker by about two to three orders of magnitude for both types of QDs. It is slightly stronger for the larger GaAs QDs. The trion wavefunctions are close, yet not equal to, single-particle states.

In conclusion, we experimentally studied negatively charged trions in two different types of semiconductor QDs and observed a radiative Auger process in the optical recombination spectrum. We employed the radiative Auger process to determine the properties of a single electron in the QD—the energy quantization and its relaxation and tunnelling dynamics—using the precise, sensitive and fast tools of quantum optics. The radiative Auger process requires only substantial Coulomb interactions within the trion, a very general feature. Therefore, this process should also occur for the positively charged trion and other quantum emitters in the solid state.

Online content

Any methods, additional references, Nature Research reporting summaries, source data, extended data, supplementary information, acknowledgements, peer review information; details of author contributions and competing interests; and statements of data and code availability are available at https://doi.org/10.1038/s41565-020-0697-2.

Received: 10 December 2019; Accepted: 22 April 2020;
Published online: 15 June 2020

References

1. Åberg, T. & Utriainen, J. Evidence for a 'radiative Auger effect' in X-ray photon emission. *Phys. Rev. Lett.* **22**, 1346–1348 (1969).
2. Åberg, T. Theory of the radiative Auger effect. *Phys. Rev. A* **4**, 1735–1740 (1971).
3. Bloch, F. & Ross, P. A. Radiative Auger effect. *Phys. Rev.* **47**, 884–885 (1935).
4. Bloch, F. Double electron transitions in X-ray spectra. *Phys. Rev.* **48**, 187 (1935).
5. Hawrylak, P. *Single Quantum Dots: Fundamentals, Applications and New Concepts* Vol. 90 (Springer Science, Business Media, 2003).
6. Bambynek, W. et al. X-ray fluorescence yields, Auger, and Coster–Kronig transition probabilities. *Rev. Mod. Phys.* **44**, 716–813 (1972).
7. Barthés-Labrousse, M.-G. The Auger effect. *Microsc. Microanal. Microstruct.* **6**, 253–262 (1995).
8. Kurzmann, A., Ludwig, A., Wieck, A. D., Lorke, A. & Geller, M. Auger recombination in self-assembled quantum dots: quenching and broadening of the charged exciton transition. *Nano Lett.* **16**, 3367–3372 (2016).
9. Han, B. et al. Exciton states in monolayer $MoSe_2$ and $MoTe_2$ probed by upconversion spectroscopy. *Phys. Rev. X* **8**, 031073 (2018).
10. Siyushev, P. et al. Optically controlled switching of the charge state of a single nitrogen-vacancy center in diamond at cryogenic temperatures. *Phys. Rev. Lett.* **110**, 167402 (2013).
11. Blood, P. *Quantum Confined Laser Devices: Optical Gain and Recombination in Semiconductors* Vol. 23 (OUP Oxford, 2015).
12. Carlson, T. A. Electron shake-off following the beta decay of Ne^{23}. *Phys. Rev.* **130**, 2361–2365 (1963).
13. Dean, P. J., Cuthbert, J. D., Thomas, D. G. & Lynch, R. T. Two-electron transitions in the luminescence of excitons bound to neutral donors in gallium phosphide. *Phys. Rev. Lett.* **18**, 122–124 (1967).
14. Skolnick, M. S. et al. Fermi sea shake-up in quantum well luminescence spectra. *Solid State Electron.* **37**, 825–829 (1994).
15. Manfra, M. J., Goldberg, B. B., Pfeiffer, L. & West, K. Anderson–Fano resonance and shake-up processes in the magnetophotoluminescence of a two-dimensional electron system. *Phys. Rev. B* **57**, R9467–R9470 (1998).
16. Kleemans, N. A. J. M. et al. Many-body exciton states in self-assembled quantum dots coupled to a Fermi sea. *Nat. Phys.* **6**, 534–538 (2010).
17. Huo, Y. H., Rastelli, A. & Schmidt, O. G. Ultra-small excitonic fine structure splitting in highly symmetric quantum dots on GaAs (001) substrate. *Appl. Phys. Lett.* **102**, 152105 (2013).
18. Warburton, R. J. et al. Optical emission from a charge-tunable quantum ring. *Nature* **405**, 926–929 (2000).
19. Hansom, J., Schulte, C. H. H., Matthiesen, C., Stanley, M. J. & Atatüre, M. Frequency stabilization of the zero-phonon line of a quantum dot via phonon-assisted active feedback. *Appl. Phys. Lett.* **105**, 172107 (2014).
20. Koong, Z. X. et al. Fundamental limits to coherent photon generation with solid-state atom-like transitions. *Phys. Rev. Lett.* **123**, 167402 (2019).
21. Brash, A. J. et al. Light scattering from solid-state quantum emitters: beyond the atomic picture. *Phys. Rev. Lett.* **123**, 167403 (2019).
22. Kouwenhoven, L. P., Austing, D. G. & Tarucha, S. Few-electron quantum dots. *Rep. Prog. Phys.* **64**, 701–736 (2001).
23. Fock, V. Bemerkung zur Quantelung des harmonischen Oszillators im Magnetfeld. *Z. Phys.* **47**, 446–448 (1928).
24. Darwin, C. G. The diamagnetism of the free electron. *Proc. Camb. Phil. Soc.* **27**, 86 (1930).
25. Ohnesorge, B., Albrecht, M., Oshinowo, J., Forchel, A. & Arakawa, Y. Rapid carrier relaxation in self-assembled $In_x Ga_{1-x}$ As/GaAs quantum dots. *Phys. Rev. B* **54**, 11532–11538 (1996).
26. Kurtze, H. et al. Carrier relaxation dynamics in self-assembled semiconductor quantum dots. *Phys. Rev. B* **80**, 235319 (2009).
27. Li, X.-Q., Nakayama, H. & Arakawa, Y. Phonon bottleneck in quantum dots: role of lifetime of the confined optical phonons. *Phys. Rev. B* **59**, 5069–5073 (1999).
28. Müller, K. et al. Probing ultrafast carrier tunneling dynamics in individual quantum dots and molecules. *Ann. Phys.* **525**, 49–58 (2013).
29. Slater, J. C. The theory of complex spectra. *Phys. Rev.* **34**, 1293–1322 (1929).
30. Bethe, H. A. & Jackiw, R. *Intermediate Quantum Mechanics* (CRC Press, 2018).

Methods

The samples were grown by molecular beam epitaxy. Sample A contained InGaAs QDs embedded in a p–i–n–i–n-diode structure[31–34]. Sample B contained GaAs QDs in AlGaAs, which were grown by GaAs infilling of Al-droplet-etched nanoholes[17,35]. The photon out-coupling was enhanced by a distributed Bragg mirror below the QDs. For both samples, the QDs were placed between a p-doped top gate and an n-type doped back gate. The QDs were tunnel-coupled to the back gate. This configuration stabilizes the charge environment of the QDs and enables tuning of the QD charge state by applying a voltage between the top gate and back gate[36,37]. For the InGaAs QDs, the back gate had a distance of 40 nm to the QDs, 30 nm for the GaAs QDs. In a magnetic field, there is optical spin-pumping in the centre of the trion charge plateau[38,39] (Supplementary Note VI). Therefore, we performed all experiments at the plateau edges, where co-tunnelling randomizes the electron spin[40].

All time-resolved measurements were performed by using superconducting single-photon detectors. The overall timing resolution (instrument response function) for the $g^{(2)}$ measurements was ~35 ps (full-width at half-maximum). Optical measurements were carried out at 4.2 K in a helium bath cryostat. Resonant excitation of the QDs was performed with a narrow-bandwidth (~1 MHz) tunable diode laser (Toptica DLpro), which was additionally filtered with a home-built grating setup to remove any background from the gain medium of the laser. Resonance fluorescence of individual QDs was measured by suppressing the reflected laser light with a cross-polarization technique.

Data availability

The data that support this work are available from the corresponding author upon reasonable request.

Code availability

The code that has been used for this work is available from the corresponding author upon reasonable request.

References

31. Löbl, M. C. et al. Narrow optical linewidths and spin pumping on charge-tunable close-to-surface self-assembled quantum dots in an ultrathin diode. *Phys. Rev. B* **96**, 165440 (2017).
32. Vora, P. M. et al. Spin-cavity interactions between a quantum dot molecule and a photonic crystal cavity. *Nat. Commun.* **6**, 7665 (2015).
33. Javadi, A. et al. Spin-photon interface and spin-controlled photon switching in a nanobeam waveguide. *Nat. Nanotechnol.* **13**, 398–403 (2018).
34. Grim, J. Q. et al. Scalable in operando strain tuning in nanophotonic waveguides enabling three-quantum-dot superradiance. *Nat. Mater.* **18**, 963–969 (2019).
35. Wang, Z. M., Liang, B. L., Sablon, K. A. & Salamo, G. J. Nanoholes fabricated by self-assembled gallium nanodrill on GaAs(100). *Appl. Phys. Lett.* **90**, 113120 (2007).
36. Patel, R. B. et al. Two-photon interference of the emission from electrically tunable remote quantum dots. *Nat. Photon.* **4**, 632–635 (2010).
37. Kiršanskė, G. et al. Indistinguishable and efficient single photons from a quantum dot in a planar nanobeam waveguide. *Phys. Rev. B* **96**, 165306 (2017).
38. Kroutvar, M. et al. Optically programmable electron spin memory using semiconductor quantum dots. *Nature* **432**, 81–84 (2004).
39. Dreiser, J. et al. Optical investigations of quantum dot spin dynamics as a function of external electric and magnetic fields. *Phys. Rev. B* **77**, 075317 (2008).
40. Smith, J. M. et al. Voltage control of the spin dynamics of an exciton in a semiconductor quantum dot. *Phys. Rev. Lett.* **94**, 197402 (2005).

Acknowledgements

We thank P. Treutlein for fruitful discussions. M.C.L., C.S. and R.J.W. acknowledge financial support from NCCR QSIT and from SNF project number 200020_156637. L.Z. received funding from the European Union Horizon 2020 Research and Innovation programme under the Marie Skłodowska-Curie grant agreement number 721394 (4PHOTON). A.J. acknowledges support from the European Unions Horizon 2020 research and innovation programme under the Marie Skłodowska-Curie grant agreement number 840453 (HiFig). J.R., A.L. and A.D.W. gratefully acknowledge financial support from the grants DFH/UFA CDFA05-06, DFG TRR160, DFG project 383065199, and BMBF Q.Link.X 16KIS0867. L.M. and P.L. gratefully acknowledge financial support from the Danish National Research Foundation (Center of Excellence Hy-Q, grant number DNRF139) and the European Research Council (ERC Advanced Grant SCALE).

Author contributions

M.C.L., C.S., L.Z., G.N.N. and A.J. performed the experiments. J.R., A.D.W. and A.L. grew the samples. C.S., M.C.L. and L.M. fabricated the different samples. M.C.L., L.Z., P.L. and A.L. designed the samples. M.C.L., C.S., L.Z. and R.J.W. analysed the data. M.C.L. developed the theory of the radiative Auger process. A.J., M.C.L. and C.S. developed the theory for the time-resolved measurements. M.C.L., R.J.W. and C.S. developed the theory for the magnetic field dispersion. M.C.L. and R.J.W. initiated the project and wrote the manuscript with input from all the authors.

Competing interests

The authors declare no competing interests.

Additional information

Supplementary information is available for this paper at https://doi.org/10.1038/s41565-020-0697-2.

Correspondence and requests for materials should be addressed to M.C.L.

Peer review information *Nature Nanotechnology* thanks Val Zwiller and the other, anonymous, reviewer(s) for their contribution to the peer review of this work.

Reprints and permissions information is available at www.nature.com/reprints.